



Photocatalytic degradation of cefotaxime pharmaceutical compounds onto a modified nanocatalyst

Noor. S. Abbood¹ · Nisreen S. Ali² · Eman H. Khader¹ · Hasan. Sh. Majdi³ · Talib M. Albayati¹ · Noori M. Cata Saady⁴

Received: 12 July 2022 / Accepted: 9 November 2022 / Published online: 15 November 2022
© The Author(s), under exclusive licence to Springer Nature B.V. 2022

Abstract

The photocatalytic advanced oxidation process as treatment for the removal of cefotaxime pharmaceutical compounds was conducted onto a modified nanocatalyst. Using photocatalysis with hydrogen peroxide (H₂O₂) in advanced oxidation processes (AOPs) is a suitable and alternative method. Therefore, this study targeted acquiring insights into using ultraviolet (UV) light radiation sources with two types of nanocatalysts (i.e., TiO₂ and TiO₂/kaolin) to reduce cefotaxime contaminants. The characterization properties of both catalysts were determined using X-ray diffraction (XRD), scanning electron microscopy (SEM), Brunauer–Emmett–Teller (BET), and Fourier-transform infrared spectroscopy (FT-IR). The study investigated the effects of the irradiation time (10–120 min), cefotaxime concentration (10–40 mg/L), TiO₂ dose (0.05–0.2 g), and pH (4–8) on the decomposition cefotaxime. The highest degradation with pure TiO₂ was obtained at a contact time of 90 min, cefotaxime concentration of 10 mg/L, TiO₂ dose of 0.2 g, and a pH of 4, with a removal efficiency of almost 68%. The results indicated that cefotaxime can easily be oxidized with a TiO₂/kaolin catalyst with a removal efficiency of approximately 99.8% when using a UV/H₂O₂ treatment. The UV/H₂O₂ oxidation was more effective and sustainable as well as being a promising technique for the treatment of cefotaxime in wastewater.

Keywords Photocatalytic degradation · Visible light photocatalysis · Wastewater treatment · Advanced oxidation · Ultraviolet irradiation · Photochemical oxidation

✉ Talib M. Albayati
Talib.M.Naieff@uotechnology.edu.iq

¹ Department of Chemical Engineering, University of Technology-Iraq, 52 Alsinaa St., Baghdad PO Box 35010, Iraq

² Materials Engineering Department, College of Engineering, Mustansiriyah University, Baghdad, Iraq

³ Department of Chemical and Petroleum Industries Engineering, Al- Mustaqbal University College, Hilla, Babylon PO Box 100, Iraq

⁴ Department of Civil Engineering, Memorial University of Newfoundland, St. John's, NL A1B 3X5, Canada

Introduction

Pharmaceutical compounds (PACs) have been released in waterways because of the inadequacy of traditional wastewater remediation plants. Pharmaceutical compounds are a type of emerging pollutant that has received much attention because of their potential risk of causing negative ecological and health effects in wildlife and humans [1, 2]. Pharmaceutical compounds and their derivatives are considered priority pollutants because they are harmful to organisms even at ppb levels. One of the most problematic aspects in trying to abate these substances is that they are often found in small concentrations in water bodies, making identification, analysis, and removal from water and wastewater treatment plants difficult [3]. Among these pharmaceuticals, cefotaxime ($C_{16}H_{17}N_5O_7S_2$) is an antibiotic used to treat several bacterial infections [4], and its chemical structure is shown in Fig. 1.

Coagulation, flocculation, chemical oxidation, membrane separation, electrochemical processes, and adsorption are some of the technologies used to remove pharmaceuticals [5–7]. The advanced oxidation process (AOP) is the most effective method for decomposing and removing persistent, resistant, and nondegradable organic contaminants in aquatic settings; thus, it has played a key role in water and wastewater treatment [8]. Advanced oxidation processes convert organic pollutants and their constituents into inorganic molecules, which are mainly harmless. The advanced oxidation process also generates hydroxyl radicals (OH^\bullet), which are powerful and very reactive oxidants that can attack almost all organic compounds. Additionally, hydroxyl radicals have a huge reaction potential (2.80 V compared to a normal hydrogen electrode) and react 10^6 – 10^{12} times faster than other oxidants, such as ozone [9].

Mainly because of its nontoxicity, physical and optical properties, high stability, and high photocatalytic activity, titanium dioxide (TiO_2) is the most commonly used and investigated catalyst [10]. On the other hand, Kaolin ($Al_2Si_2O_5(OH)_4$) is a 1:1 clay mineral composed of stacked layers of SiO_4 tetrahedral sheets and $AlO_2(OH)_4$ octahedral sheets, that usually exhibits various morphologies, including a two-dimensional morphology (nanoflakes) and a one-dimensional morphology (nanotubes and nanorods) [11]. Meanwhile, kaolin clays have many hydroxyl groups on their surfaces, which helps with surface modification and makes kaolin a good matrix for anchoring TiO_2 particles to boost the photocatalytic activity. The kaolin matrix may modulate the crystal type of TiO_2 particles, thereby improving

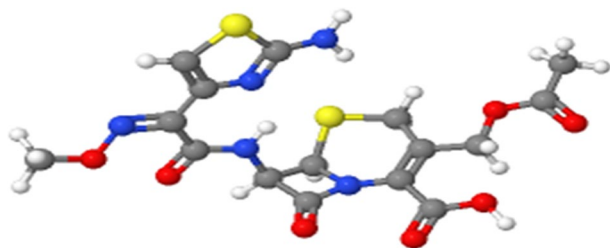


Fig. 1 Chemical structure of cefotaxime

catalytic performance [12]. The UV/H₂O₂ system is considered advantageous when employed in the advanced oxidation process because it results in a smaller footprint in the treatment plant due to its high reaction rates and flexibility in reactor design. Because of the lower cost and easy availability of hydrogen peroxide, this method for advanced oxidation process treatment is less costly [13].

As indicated above, no research has been done on the advanced oxidation process of cefotaxime from aquatic environments by nanocatalyst (i.e., TiO₂ and TiO₂/kaolin) with the addition of UV/H₂O₂; so the goal of this study is the application of two types of powder catalysts (i.e., TiO₂ and TiO₂/kaolin) they prepared and characterized for the photocatalytic degradation of cefotaxime contaminants with the addition of UV/H₂O₂. The structure and performance differences between the pure TiO₂ and composite TiO₂/kaolin were determined by various characterizations using X-ray diffraction (XRD), scanning electron microscopy (SEM), Brunauer–Emmett–Teller (BET) surface area, and Fourier-transformed infrared spectra (FT-IR). Furthermore, this study investigated the effect of the irradiation time, catalyst dose (TiO₂/kaolin/H₂O₂), initial concentration of cefotaxime, and pH on the degradation of cefotaxime pharmaceutical compounds.

Materials and methods

Materials

Sodium chloride (NaCl, Mwt.=58.443 g/mol), titanium dioxide (TiO₂, purity ≥99%), sulfuric acid (H₂SO₄, purity 99%), and hydrogen peroxide (H₂O₂, 30% solution (w/w) in H₂O) were purchased from Sigma-Aldrich Company as well as cefotaxime (1 g) from PHIL Inter Pharma (USA). The kaolin clay (particle size = 0.06 mm) used in the present research was obtained from the Ministry of Industry and Minerals/Iraq Geological Survey, Baghdad, Iraq. The chemical composition of the sample was SiO₂ 48.7%, Al₂O₃ 34.8%, Fe₂O₃ 1%, MgO 0.07%, CaO 0.31%, Na₂O 0.13%, K₂O 0.15%, TiO₂ 3.5%, and loss on ignition. The UV and visible irradiances at the reactor surface were 0.16 W/m² (Philips 16 W/G16 T8, Holland) and 15 W/m² (Philips 20 W/60 1M7 India), respectively.

Characterization

X-ray powder diffraction (XRD) tests were conducted with a diffraction unit (Shimadzu-6000, Japan) at the Nano Technology Center/University of Technology. Using a scanning electron microscope (SEM) (VEGA 3 LM, Germany) available at the Central Service Laboratory (College of Education for Pure Sciences/Ibn Al Haitham/Baghdad University), a morphological analysis of the catalysts (i.e., TiO₂ and TiO₂/kaolin) was performed. The specific surface area and total pore volume of the catalysts (i.e., TiO₂ and TiO₂/kaolin) were measured using a Brunauer–Emmett–Teller (BET) surface area analyzer (Q-surf 9600, USA) from the Petroleum Research and Development Center (Baghdad). A Fourier-transformed

infrared (FT-IR) spectrophotometer (Bruker Tensor 27, Germany) with a range from 500 to 4000 cm^{-1} recorded the FT-IR spectra.

Photocatalytic activity

The photocatalytic degradation of cefotaxime was used to evaluate the photocatalytic performance of the prepared samples. The examination setup included a batch reactor with a magnetic stirrer and two ultraviolet (UV) lamps (wavelength = 254 nm) in a batch system. During the experiment, the entire assembly was kept in a darkroom to eliminate the influence of any ambient light and to ensure that the photocatalytic degradation of cefotaxime occurred solely under the irradiation from the light source used. To attain complete adsorption–desorption equilibrium, the mixture of the catalyst and wastewater was stirred vigorously and stored in the dark for 30 min before turning on the lamp. As soon as the equilibrium state is reached, the lights are turned on. To remove the catalyst, 10 ml of sample was withdrawn, centrifuged, and filtrated by nanofiltration. After filtration, it was stored in 4-mL glass vials and sent for high-performance liquid chromatography (HPLC) analysis (Agilent 1100/1200 HPLC, to quantify the cefotaxime. Using the following equation, the percentage removal of cefotaxime was calculated [14]:

$$\% \text{Removal of cefotaxime} = \frac{(C_i - C_o)}{C_i} * 100 \quad (1)$$

where c_i = initial concentration of cefotaxime and c_o = final concentration of cefotaxime.

Results and discussion

Characterization of the catalyst

Figure 2 displays the spectroscopic structures of TiO_2 , kaolin, and the TiO_2 /kaolin composite that were analyzed by X-ray diffraction (XRD), and as shown in Fig. S1 as well. The crystal planes of the TiO_2 [(101), (004), (200), (105), (211), and (204)] that appeared in the pure TiO_2 , and TiO_2 /kaolin composite agreed with the characteristic peaks of TiO_2 at 25.36°, 37.84°, 48.12°, 53.96°, 55.16°, and 62.76°, respectively [15]. After the addition of kaolin, the grain sizes of the TiO_2 decreased significantly from 30 to 14 nm. The grain size of the loaded TiO_2 nanoparticles was controlled efficiently by the addition of kaolin, which enhanced the photoactivity.

Figure 2 clearly illustrates the (001) diffraction peak of kaolin at 12.28° displayed by the XRD pattern of kaolin, indicating a d spacing of 0.72 nm, which corresponds well to the standard pattern (JCPDS No.14-0164). In addition, the peaks at 24.82°, 38.34°, and 62.26° corresponded to the (002), (−202), and (060) lattice planes of triclinic kaolin. In the TiO_2 /kaolin composite, the characteristic peaks of kaolin disappeared, which could be attributed to the completion of the dehydroxylation reaction [16].

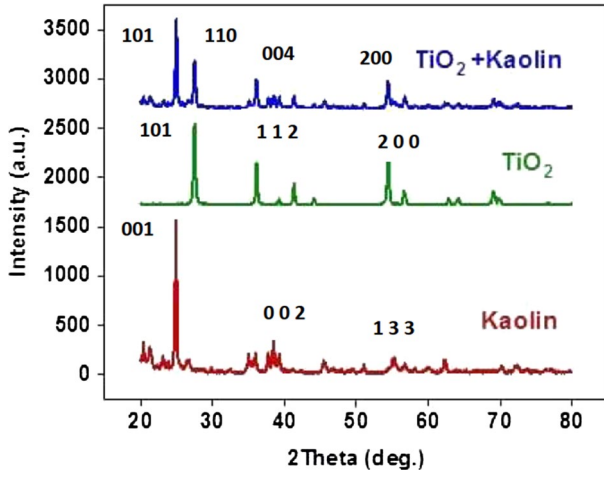


Fig. 2 XRD images of TiO₂, kaolin, and TiO₂/kaolin

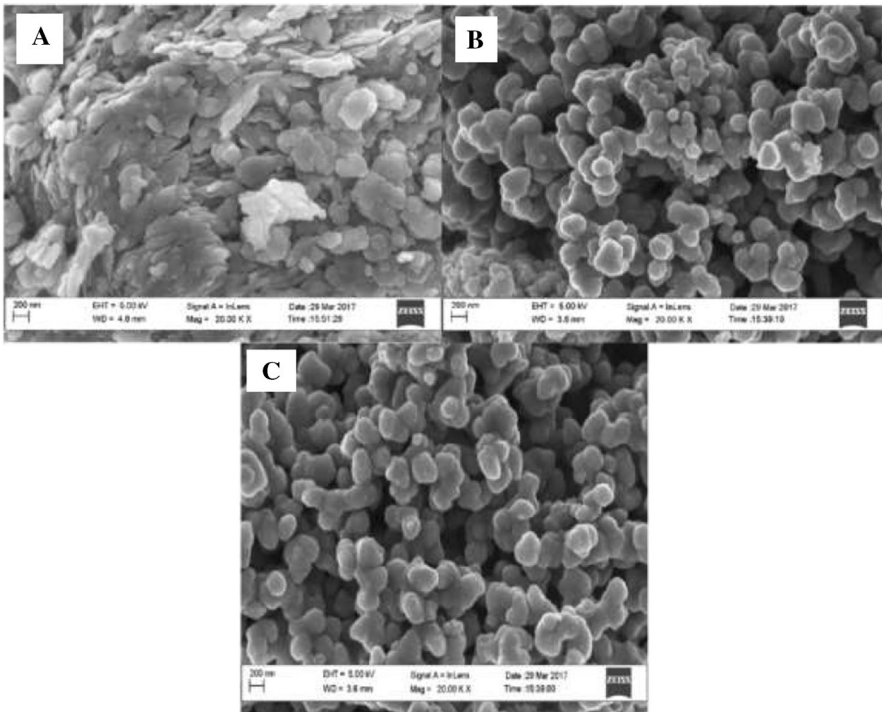


Fig. 3 SEM images of A TiO₂ B kaolin C TiO₂/kaolin

The general morphologies and microstructures of TiO_2 , kaolin, and $\text{TiO}_2/\text{kaolin}$, were investigated by SEM analysis, as shown in Fig. 3. The surface morphology of TiO_2 is displayed in Fig. 3a. Spherical nanoparticles were revealed in the SEM image of TiO_2 (Fig. 3a), repeating the same observations of TiO_2 morphology reported by the reference [17]. Kaolin exhibited layered structures consisting of several parallel nanosheets, as indicated in Fig. 3b. The assembly of the TiO_2 particles was significantly promoted by the kaolin, which has a smooth and regular surface without impurities.

Figure 3c demonstrates that the problems of agglomeration and high surface energy when using pure TiO_2 were resolved by using the $\text{TiO}_2/\text{kaolin}$ composite. From this image, it is apparent that TiO_2 particles covered the originally smooth edges of the kaolin plates (see Fig. 3b) in the case of the $\text{TiO}_2/\text{kaolin}$ composite. Figure 3c shows that the TiO_2 nanoparticles grew preferably on the kaolin particle edges. This means that the solid, smooth surface of the kaolin particles with no cracks is not compatible with the development of TiO_2 nanoparticles. However, the results of Chong et al. contradict these conclusions [18].

The surface area and pore volume were investigated by Brunauer–Emmett–Teller (BET) analysis to understand the roles of both TiO_2 and kaolin in the $\text{TiO}_2/\text{kaolin}$ composite. As indicated in Table 1, the specific surface area and total pore volume of TiO_2 and kaolin are smaller than those of the $\text{TiO}_2/\text{kaolin}$ composite. The homogeneous distribution of nano- TiO_2 particles and the unique creation of a kaolin-layered structure could explain the huge surface area and total pore volume of the $\text{TiO}_2/\text{kaolin}$ composite. Kaolin composite can efficiently upgrade the improvement of the catalytic activity by creating more adsorption and reactive sites.

One of the most effective experimental methods for researching hydrogen-bonded clusters is vibrational spectroscopy [19]. The FT-IR spectra of the samples, shown in Fig. 4 and Fig. S2 (A, B, and C), were used to analyze the vibrational bands and interface interactions. The obvious Ti–O–Ti stretching vibration in the range of $699\text{--}732\text{ cm}^{-1}$ was displayed by all three samples, as can be seen [20], while the stretching vibration of the hydroxyl bonds appeared on the region of the broad peaks within the range from $3100\text{ to }3600\text{ cm}^{-1}$. Due to surface-adsorbed water molecules, the peak at 1630 cm^{-1} can be assigned to an H–O–H bending vibration. Photocatalytic activity is promoted by hydroxyl bonds from such adsorbed water molecules, which form the hydroxyl radical (OH^\bullet) and are categorized as an oxidant because they react with a photo-induced hole (h^+) or oxygen (O_2) [21]. The band within the wavenumber range from $1007\text{--}1115\text{ cm}^{-1}$ can be assigned to the Si–O stretching vibration for the kaolin as well as the $\text{TiO}_2/\text{kaolin}$ composite, while the stretching

Table 1 Physicochemical properties of TiO_2 and supported catalysts

No	Sample	S_{BET} (m^2/g)	Pore volume (cm^3/g)
1	TiO_2	282.8	0.64
2	Kaolin	89.8	0.38
3	$\text{TiO}_2/\text{kaolin}$	368.7	0.76

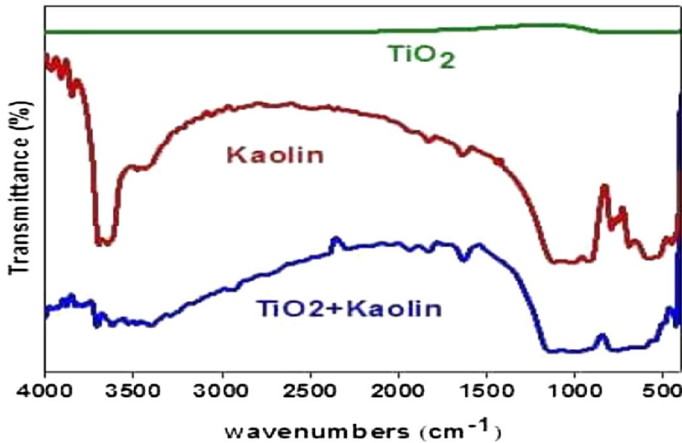


Fig. 4 FT-IR images of TiO_2 , Kaolin, and $\text{TiO}_2/\text{kaolin}$

of the Si–O appeared at a peak at 697 cm^{-1} [22]. The Si–O–Al stretching vibration can be seen at the peaks near wavenumbers 537 , 754 , and 793 cm^{-1} [23]. The peak at 3621 cm^{-1} indicated the occurrence of –OH stretching, while the bending vibrations of the adsorbed water led to the peak occurring at around 1639 cm^{-1} [24]. The peaks appearing at 913 and 3697 cm^{-1} displayed the presence of Al–OH vibrations caused by the alumina sheet of kaolin coordinated with –OH groups [25]. Also, at 3653 cm^{-1} , the Al–OH bond materialized as an octahedral structure. Additionally, due to the presence of TiO_2 and caused by the replacement of aluminum ions with titanium ions, this peak disappeared in the $\text{TiO}_2/\text{kaolin}$ composite. The band positions at $\sim 755\text{ cm}^{-1}$, 696 cm^{-1} , and 539 cm^{-1} are part of the Si–O–Al vibrations [26].

Photocatalytic degradation of cefotaxime

Effect of the irradiation time

Figure 5 displays the outcomes of the effect of the irradiation time on the cefotaxime removal with pure TiO_2 and with a mixture of $\text{TiO}_2/\text{kaolin}/\text{H}_2\text{O}_2$ under UV light, showing that the removal efficiency increased as the irradiation time increased. This occurred because over time, more cefotaxime adsorbed to the catalyst surface, which caused more cefotaxime to degrade [27]. With time, the generation of radicals was higher, and that caused an increase in the degradation rate [28]. The removal efficiency was 55.69% at 90 min when using TiO_2 only, while the removal efficiency was 94.2% at 90 min when combining $\text{TiO}_2/\text{kaolin}/\text{H}_2\text{O}_2$.

The addition of kaolin and hydrogen peroxide to the catalyst improved the photocatalytic performance by up to 1.7 times when compared to using pure TiO_2 . This improved performance was due to the optimized conditions: increased surface area, porous nature, and TiO_2 phase. The additional cefotaxime molecules adsorbed on the larger surface area, which increased the photodegradation activity. The adsorbed pollutant on the surface of the kaolin was continuously degraded by TiO_2 , where

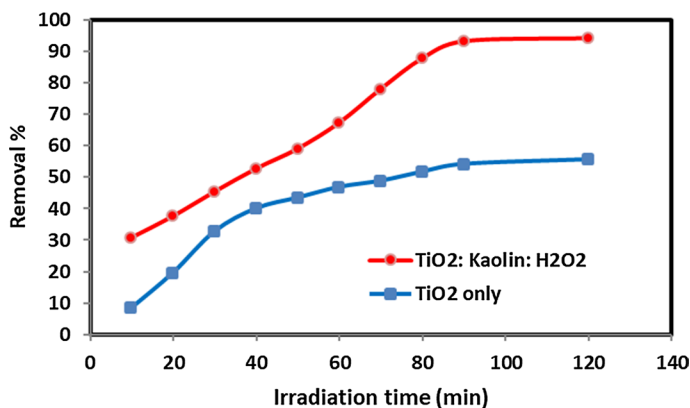


Fig. 5 Effect of irradiation time on the removal efficiency of cefotaxime ($\text{TiO}_2=0.1 \text{ g}/0.5 \text{ L}$, $\text{TiO}_2/\text{kaolin}/\text{H}_2\text{O}_2=0.1:0.2:0.05 \text{ g}$, $\text{pH}=7$, cefotaxime concentration = 10 ppm)

the kaolin adsorbed the pollutant on its external surfaces and within its interlinear portions [29]. When TiO_2 is bombarded with enough photon energy, electrons and holes are generated, which initiate the cefotaxime photodegradation pathway [30]. The electron will be promoted to the conduction band, while the hole will remain in the valence band. Both the electron and the hole produce hydroxyl radicals when they combine with oxygen and water, respectively [31]. These hydroxyl radicals (powerful oxidizing agents) target the cefotaxime and convert it to various compounds, such as NO_3 , NH^{+4} , SO_4^{-2} , and CO_2 [32].

Effect of the catalyst dose

By loading different amounts of TiO_2 and $\text{TiO}_2/\text{kaolin}/\text{H}_2\text{O}_2$ during the photocatalytic reaction, the effect of the catalyst dose was also studied, where the irradiation time (90 min) and cefotaxime concentration (10 mg/L) were kept constant. The photodegradation of the cefotaxime increased with additional amounts of TiO_2 (see Fig. 6) and then decreased. With the catalyst amount (TiO_2) equal to 0.1 g, the most effective removal efficiency of cefotaxime (54.2%) was observed. An increase in the TiO_2 amount increased the number of active sites (but only to a certain limit), which in turn increased the number of hydroxyl and superoxide radicals, resulting in the enhanced photodegradation of cefotaxime. Due to the interception of light by suspension that resulted from increasing the amount of TiO_2 above the optimum limit, the degradation rate remained reduced after reaching that limit. This can be explained by the agglomeration of TiO_2 catalyst particles whose surfaces became unavailable for photon absorption [33].

To establish the appropriate amount of photocatalyst ($\text{TiO}_2/\text{kaolin}/\text{H}_2\text{O}_2$), a series of tests were conducted with varying amounts of that photocatalyst, ranging between 0.05 and 0.2 g/0.5 L of the solution. Figure 7 shows the results of these experiments. The removal efficiency of cefotaxime reached 54.2% using 0.1 g TiO_2 only, 60.8% using 0.1 g $\text{TiO}_2:0.1 \text{ g}$ kaolin, and 62.27% using 0.1 g $\text{TiO}_2:0.025 \text{ g}$ H_2O_2 . The

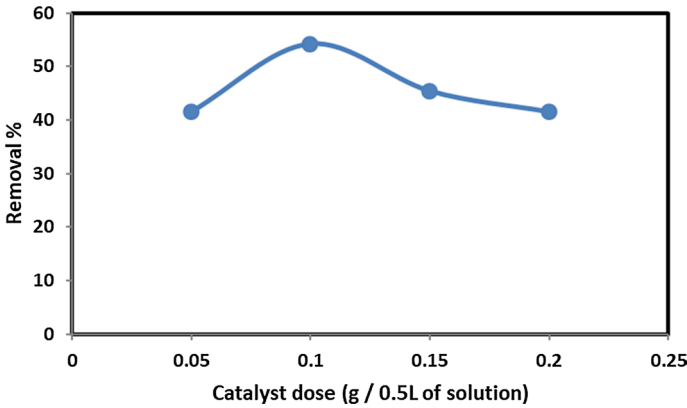


Fig. 6 TiO₂ dose effect on the removal efficiency of cefotaxime (irradiation time=90 min, cefotaxime concentration = 10 ppm, pH=7)

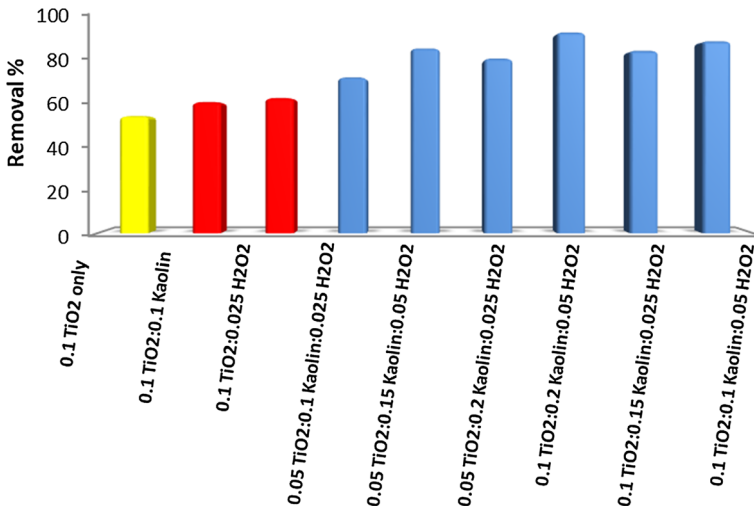


Fig. 7 Effect of TiO₂/kaolin/H₂O₂ dose on the removal efficiency (irradiation time=90 min, cefotaxime concentration = 10 ppm, pH=7)

highest removal efficiency of cefotaxime was observed to be 93.2% with the catalyst amount equal to 0.1:0.2:0.05 g of TiO₂/ kaolin/H₂O₂, respectively. At these optimal levels, the surface chemical interaction, ternary catalyst molecular architecture, and morphological features formed the best aqueous environment for the efficient interaction with the cefotaxime molecules [34]. The degree of degradation of the cefotaxime solution increased with an increasing amount of photocatalyst, reached a higher value, and then decreased. This is could be attributed to the shielding effect, where the suspended TiO₂/kaolin/H₂O₂ particles reduced the penetration of light through the solution after exceeding the optimal amount [35].

Effect of the cefotaxime concentration

The results obtained from the effect of the initial cefotaxime concentration on the removal efficiency of cefotaxime are shown in Fig. 8. The cefotaxime concentration was varied from 10 to 40 ppm, but the other amounts remained constant at TiO_2 (0.1 g), $\text{TiO}_2/\text{kaolin}/\text{H}_2\text{O}_2$ (0.1:0.2:0.05 g), and $\text{pH}=7$. Figure 8 reveals that as the cefotaxime concentration rose, the removal efficiency decreased. This behavior occurred because more organic substances adsorbed on the surface of the catalyst as the cefotaxime concentration increased, while fewer $\bullet\text{OH}$ groups were formed because fewer photons were available to reach the catalyst surface, which lowered the degradation percent [36]. The highest removal efficiency when using TiO_2 only was 54.2%, while with the addition of kaolin and hydrogen peroxide, the removal efficiency increased to 93.2%, as seen in Fig. 8.

Effect of the pH

Figure 9 shows the effect of the pH on the removal efficiency of cefotaxime, indicating that the cefotaxime removal efficiency decreased as the pH of the solution increased.

The optimum removal was 67.9% at a pH of 4 using TiO_2 only but 99.83% by combining $\text{TiO}_2/\text{kaolin}/\text{H}_2\text{O}_2$. This was due to the H_2O_2 modifying the prevailing electric charge on the TiO_2 and kaolin surfaces. Because the pH value was lower than the zero point of charge (ZPC) of the pH (e.g., $\text{pH}=4$), there was more pollutant adsorption on the TiO_2 surface as a result of the positive electric charge on that surface. Additionally, because a hydroxyl free radical was created as a result of the catalyst surface stimulation, higher adsorption of the pollutant on its surface induced radicals (made at the catalyst surface) that more quickly impacted the cefotaxime molecules and removed them [37]. This special property of H_2O_2 could be the reason for the lower performance of the $\text{TiO}_2/$

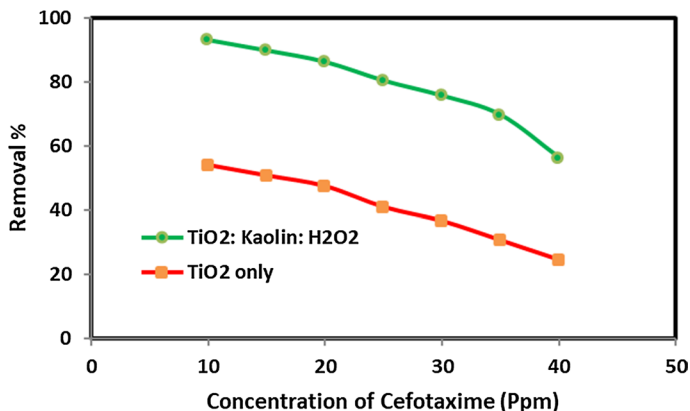


Fig. 8 Effect of cefotaxime concentration on the removal efficiency ($\text{TiO}_2 = 0.1 \text{ g} / 0.5 \text{ L}$, $\text{TiO}_2/\text{kaolin}/\text{H}_2\text{O}_2 = 0.1:0.2:0.05 \text{ g}$, irradiation time = 90 min, $\text{pH}=7$)

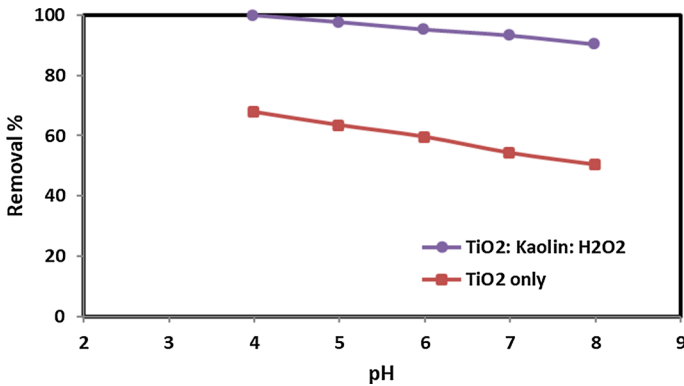


Fig. 9 Effect of pH on the removal efficiency of cefotaxime ($\text{TiO}_2=0.1 \text{ g} / 0.5 \text{ L}$, $\text{TiO}_2/\text{kaolin}/\text{H}_2\text{O}_2=0.1:0.2:0.05 \text{ g}$, irradiation time = 90 min, cefotaxime concentration = 10 ppm)

kaolin/ H_2O_2 at higher pH levels. On the other hand, the H_2O_2 (which is strongly dependent on the pH) becomes highly unstable, and self-decomposition of H_2O_2 occurs in an alkaline medium [38]. The H_2O_2 molecules will rapidly break down into water and oxygen as a result of this self-decomposition, and the molecule will lose its characteristics as an oxidant and mainly become the source of hydroxyl radicals. Thus, the cefotaxime removal efficiency will decrease. Therefore, the reports that concluded that the photocatalysis process can remove pollutants under both acidic and neutral conditions are consistent with these results [39]. At an acidic range (pH = 4–6), cefotaxime removal by a $\text{TiO}_2/\text{kaolin}/\text{H}_2\text{O}_2$ adsorbent was more effective because more protons were available at the low pH values. This resulted in an increase in the electrostatic attraction between the positive charge on the $\text{TiO}_2/\text{kaolin}/\text{H}_2\text{O}_2$ surface and the negatively charged cefotaxime anions, which increased the cefotaxime adsorption capacity. Such results have also been reported by [40], which is compatible with the results of this research.

Comparative study

The elimination of the cefotaxime compound was the subject of this research using pure TiO_2 and TiO_2 combined with kaolin with the assistance of UV/ H_2O_2 in a photocatalytic advanced oxidation process. In the actual wastewater treatment, the photocatalytic process was performed to obtain the highest removal efficiency of the cefotaxime compound because this process generates highly reactive intermediates that increase the activity of the process, thus increasing the removal of cefotaxime. In addition, it is an automatic and safe process. Table 2 compares this study to others related to the elimination of the cefotaxime component by the photocatalytic method.

Table 2 Comparison between this study and other studies

No	Catalyst	Removal	Advance oxidation process conditions	References
1	Mesoporous carbon nitride (MCN)	99%	initial cefotaxime solution concentration $C_0 = 2 \text{ mg/L}$, adsorbent dose = 150 mg, pH = 3.0, time = 30 min	[41]
2	Graphitic carbon nitride ($\text{g-C}_3\text{N}_4$)	98.4%	initial cefotaxime solution concentration $C_0 = 10 \text{ ppm}$, time = 25 min	[42]
3	Ti/CNT/SnO ₂ -Sb-Er	81.6%	initial cefotaxime solution concentration $C_0 = 50 \text{ ppm}$, pH 7.0, time = 4 h	[43]
4	titanium dioxide (TiO ₂)	84.2%	TiO ₂ initial concentration = 2.5 g/L at pH = 8.5, time = 80 min	[44]
	Zinc oxide (ZnO)	90.6%	ZnO initial concentration = 1.7 g/L at pH = 8.5, temperature = 35 °C, time = 80 min	
5	TiO ₂ /kaolin/H ₂ O ₂	99.8%	TiO ₂ /kaolin/H ₂ O ₂ = 0.1:0.2:0.05 g, pH 7.0., temperature = 25 °C time = 90 min	This study

Conclusions

The present study showed the applicability of an advanced oxidation process in the treatment of wastewater. Parameters, such as the irradiation time, cefotaxime concentration, catalyst (i.e., TiO₂, kaolin) dose, and pH, affected the removal of the cefotaxime compound. The results showed that combining TiO₂ with kaolin and H₂O₂ as catalysts led to an almost complete reduction of the cefotaxime. Combining TiO₂ with kaolin and H₂O₂ was more effective compared to utilizing only TiO₂ in the removal of cefotaxime from wastewater. The highest cefotaxime removal was 99.83% by TiO₂ combined with kaolin and H₂O₂ (0.1:0.2:0.05) g, and 68% using 0.2 g of only TiO₂. Each of these processes required an irradiation time of 90 min at a pH of 4 and a cefotaxime concentration of 10 ppm. Based on the results, an advanced oxidation process employing combined catalyst technology is appropriate for the treatment of cefotaxime in wastewater.

Supplementary Information The online version contains supplementary material available at <https://doi.org/10.1007/s11164-022-04879-3>.

Acknowledgements The authors wish to thank the Department of Chemical Engineering, University of Technology- Iraq, Baghdad, Iraq, Mustansiriyah University/College of Engineering/Materials Engineering Department Baghdad-Iraq, and Department of Chemical and Petroleum Industries Engineering, Al-Mustaqbal University College, Babylon, Iraq.

Authors' contribution All authors have contributed to this manuscript.

Funding Not applicable.

Declarations

Conflict of interest The authors declare that they have no competing interests.

References

1. N.A. Atiyah, T.M. Albayati, M.A. Atiya, *J. Molecule Struct.* **1260**, 132879 (2022)
2. N.A. Atiyah, T.M. Albayati, M.A. Atiya, *Adv. Powder Technol.* **33**(2), 103417 (2022)
3. E.H. Khader, T.J. Mohammed, T.M. Albayati, *Desalination Water Treat.* **229**, 372 (2021)
4. X. Ruan, X. Cui, Y. Cui, X. Fan, Z. Li, T. Xie, K. Ba, G. Jia, H. Zhang, L. Zhang, W. Zhang, X. Zhao, J. Leng, S. Jin, D.J. Singh, W. Zheng, *Adv. Energy. Mat.* **12**(16), 2200298 (2022)
5. A.T. Khadim, T.A. Albayati, *Cata Saady Env. Nano. Moni. & Manag.* **17**, 100635 (2022)
6. S.T. Kadhum, G.Y. Alkindi, T.M. Albayati, *T.M. Int. J. Env. Sci. Tech.* **19**(3), 1383 (2022)
7. S.M. Alardhi, J.M. Alrubaye, T.M. Albayati, *I.O.P. Conf. Ser.: Mater. Sci. Eng.* **928**, 052020 (2020)
8. M.M. Fazilati, *Desalination Water Treat.* **169**, 222 (2019)
9. R. Liang, A. Hu, W. Li, Y.N. Zhou, *J. Nano. Res* **15**(10), 1 (2013)
10. G. Jia, Y. Wang, X. Cui, W. Zheng, *ACS Sustain. Chem. Eng.* **6**(10), 13480 (2018)
11. X. Li, A. Tang, *RSC Adv.* **6**, 15585 (2016)
12. X. Li, J. Ouyang, Y. Zhou, H. Yang, *Sci. Rep.* **5**, 13763 (2015)
13. S. Krishnan, H. Rawindran, C.M. Sinnathambi, J.W. Lim, *IOP Conf. Ser.: Mater. Sci. Eng.* **206**, 012089 (2017)
14. N.S. Ali, N.M. Jabbar, S.M. Alardhi, H.S. Majdi, T.M. Albayati, *Heliyon* **8**(8), e10276 (2022)
15. C. Li, Z. Sun, Y. Xue, G. Yao, S. Zheng, *Advan. Pow. Tech.* **27**, 330 (2016)

16. S. Mustapha, J.O. Tijani, M.M. Ndamitso, A.S. Abdulkareem, D.T. Shuaib, A.K. Mohammed, *Env. Nano. Moni. & Manag.* **15**, 100414 (2021)
17. N.S. Ali, Z.T. Alismaeel, H.S. Majdi, N.M. Cata Saady, T.M. Albayati, T.M. Heliyon, *Heliyon* **8**(6), e09737 (2022)
18. M.N. Chong, V. Vimonses, S. Lei, B. Jin, C. Chow, C. Saint, *Micro. Meso. Mater.* **117**, 233 (2009)
19. Y.C. Yen, S. Ou, K.J. Lin, *J. Chin. Chem. Soc.* **64**, 1392 (2017)
20. X. Cheng, X. Yu, Z. Xing, L. Yang, *Arab. J. Chem.* **9**, S1706 (2016)
21. J. Henych, V. Stengl, *Clay Miner.* **61**, 165 (2013)
22. A.K. Panda, B.G. Mishra, D.K. Mishra, R.K. Singh, *Eng. Asp.* **363**, 98 (2010)
23. S.B. Rekik, S. Gassara, J. Bouaziz, A. Deratani, S. Baklouti, *Appl. Clay Sci.* **143**, 1 (2017)
24. N.H. Mohtor, M.H.D. Othman, A.F. Ismail, M.A. Rahman, J. Jaafar, N.A. Hashim, *Environ. Sci. Pollut. R.* **24**, 15905 (2017)
25. M. Naghsh, K. Shams, *Appl. Clay Sci.* **146**, 238 (2017)
26. A. Mishra, A. Mehta, M. Sharma, S. Basu, *J. Alloys Compd.* **694**, 574 (2016)
27. K.M. Kutlakova, J. Tokarsky, P. Kovar, S. Vojteskova, A. Kovarova, B. Smetana, J. Kukutschova, P. Capkova, V. Matejka, *J. Haz. Mat.* **188**, 212 (2011)
28. F. Amiri, M. Dehghani, Z. Amiri, S. Yousefinejad, A. Azhdarpoor, *Water Sci. Tech.* **83**(12), 3110 (2021)
29. A. Alam, D. Saha, S.C. Dey, M. Mominur, *J. Mater. Environ. Sci.* **11**(11), 1828 (2020)
30. Y. Li, S.G. Li, J. Wang, Y. Li, C.H. Ma, L. Zhang, *Russian. J. Phys. Chem. A* **88**, 2471 (2014)
31. H. Xu, S. Sun, S. Jiang, H. Wang, R. Zhang, Q. Liu, *J. Sol Gel Sci. Technol.* **87**, 676 (2018)
32. G. Mamba, X.Y. Mbianda, A.K. Mishra, *Environ. Sci. Pollut. Res.* **21**(8), 5597 (2014)
33. J. Grzechulska, A.W. Morawski, *Environment* **36**(1), 45 (2002)
34. S.D. Marathe, V.S.S. Hrivastava, *Adv. Appl. Sci. Res.* **4**(6), 212 (2013)
35. S. Rahimi, M.H. Ehrampoush, M.T. Ghaneian, S. Reshadat, A. Fatehizadeh, M. Ahmadian, G. Ghaneizadeh, *J. Chem.* **25**(13), 7427 (2013)
36. S.Y. Hashemi, M.Y. Badi, H. Pansolar, A. Azari, H. Arfaeina, A. Kiani, *Int. J. Environ. Anal. Chem.* **25**, 871 (2020)
37. C.Y. Chan, S. Tao, R. Dawson, P.K. Wong, *Environ. Pollut.* **131**, 45 (2004)
38. J. Chen, L. Zhu, *Cata. Today.* **126**(3–4), 463 (2007)
39. S.F. Kang, C.H. Liao, S.T. Po, *Chemistry* **41**(8), 1287 (2001)
40. M.Y. Badi, A. Esrafil, H. Pasalari, R.R. Kalantary, E. Ahmadi, M. Gholami, A. Azari, *Environ. Heal. Sci. Eng.* **17**(2), 685 (2019)
41. M. Dou, J. Wang, B. Gao, C. Xu, F. Yang, *Chem. Eng. J.* **383**, 123134 (2020)
42. B. Gao, J. Wang, M. Dou, X. Huang, X. Yu, *Sep. Puri. Tech.* **241**, 116576 (2020)
43. J. Lei, P. Duan, W. Liu, Z. Sun, X. Hu, *Chemistry* **250**, 126163 (2020)
44. D.E. León, H. Zúñiga-Benítez, G.A. Peñuela, *Water Air, & Soil Poll.* **228**(9), 1 (2017)

Publisher's Note Springer Nature remains neutral with regard to jurisdictional claims in published maps and institutional affiliations.

Springer Nature or its licensor (e.g. a society or other partner) holds exclusive rights to this article under a publishing agreement with the author(s) or other rightsholder(s); author self-archiving of the accepted manuscript version of this article is solely governed by the terms of such publishing agreement and applicable law.